IJE TRANSACTIONS A: Basics Vol. 39, No. 10, (October 2026) 2617-2629

International Journal of Engineering

Journal Homepage: www.ije.ir

Demagnetization Study of Permanent Magnets During the Startup of LSPMSM Considering the Effects of Temperature

L. Anh Tuan[a], T. Duy Khanh[b], N. Y. Do*[c]

[a] *School of Electrical and Electronic Engineering, Hanoi University of Industry, Hanoi, Vietnam*
[b] *Faculty of Electrical Engineering, Saodo University, Haiphong, Viet Nam*
[c] *Faculty of Electro-Mechanics, Hanoi University of Mining and Geology, Hanoi, Vietnam*

P A P E R I N F O

Paper history:
Received 14 August 2025
Received in revised form 31 December 2025
Accepted 07 January 2026

Keywords:
Demagnetization
Permanent Magnet
Temperature
Line-start Permanent Magnet Synchornous Motor
Electric Motor

A B S T R A C T

The line-start permanent magnet synchronous motor (LSPMSM) is increasingly being applied due to its high efficiency. However, temperature has a significant effect on the electromagnetic parameters, which in turn affects the operating characteristics of the LSPMSM. Due to the presence of squirrel-cage components in the rotor, LSPMSM can line-start, but the high starting current can lead to localized or complete demagnetization, especially at elevated temperatures. This can result in irreversible demagnetization of the permanent magnets. This paper analyzes the effect of temperature on the electromagnetic parameters of the motor as well as its impact on demagnetization during LSPMSM startup. The theoretical study results indicate the influence of temperature on the electromagnetic parameters of LSPMSM and demonstrate that, under certain temperature conditions, there exists a maximum starting current coefficient to prevent demagnetization. Using FEA simulation for a LSPMSM, 15kW, 2p=2, results show a correlation between theoretical and simulated findings. It is shown that with a high starting current of 337.8A, NdFeB-N38M magnets used in the motor can experience mild demagnetization at 60°C, while visible demagnetization occurs at 120°C. Experimental validation has confirmed the accuracy, as the B-EMF characteristics indicate a close resemblance between experimental and simulated results, with a deviation of less than 7%.

***doi**: 10.5829/ije.2026.39.10a.21*

Graphical Abstract

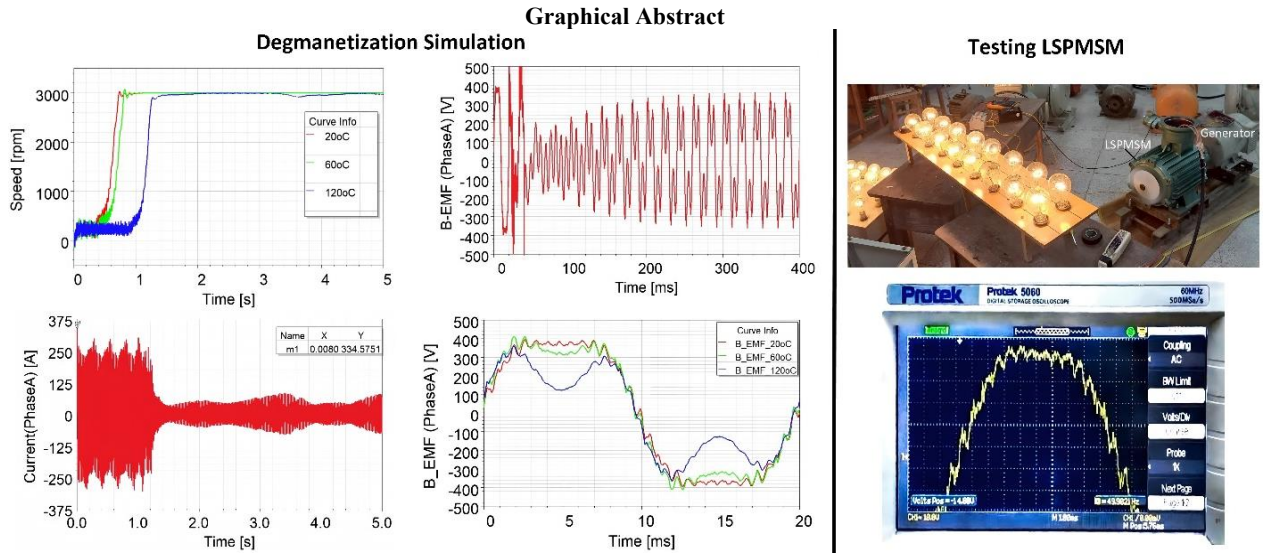

*Corresponding Author Email: donhuy@humg.edu.vn (N. Y. Do)

Please cite this article as: Anh Tuan L, Duy Khanh T, Do NY. Demagnetization Study of Permanent Magnets During the Startup of LSPMSM Considering the Effects of Temperature. International Journal of Engineering, Transactions A: Basics. 2026;39(10):2617-29.

1. INTRODUCTION

Recently, the line-start permanent magnet synchronous motor (LSPMSM) has been widely investigated and applied as a type of permanent magnet synchronous motor (PMSM). This motor offers several advantages, including high efficiency, self-starting capability upon power supply, reliable operation, and low operating costs (1). Additionally, the trend of applying LSPMSM in manufacturing is driven by the need for motors to meet increasingly stringent efficiency standards for electric motors. In fact, many energy efficiency regulations and energy policies have been enacted, such as the IEC 60034-30-1:2014 standard issued by the International Electrotechnical Commission in June 2014, which specifies the energy efficiency levels for electric motors (2).

However, the long-term operational efficiency of LSPMSM, as well as PMSM, significantly depends on electromagnetic parameters such as d-axis and q-axis synchronous inductances (L_{md}, L_{mq}), leakage inductance (L_{ls}), stator winding resistance (R_s), and remanence of permanent magnet (PM) (B_r) (3). These parameters are strongly influenced by temperature, especially in industrial applications where the motor operates under conditions of significant variations in ambient temperature and load temperature (4). When the operating temperature of the motor is high, it reduces the remanence and coercive force (H_c) of the PM, leading to a decline in parameters such as rotor flux, torque, efficiency, power factor, and so on (5-7).

The demagnetization phenomenon of PMs refers to the reduction of magnetic strength in PMs, which typically occurs when the temperature exceeds the operational limits or when the PMs are subjected to strong opposing magnetic fields (8-10). In LSPMSM, irreversible demagnetization (ID) can occur in two stages. During startup, the large starting current generates a significant opposing magnetic field, combined with the rapid increase in rotor temperature due to Joule losses in the squirrel cage (4, 11). In steady-state operation, high ambient temperatures or prolonged heavy loading can significantly raise the rotor temperature (10). Adly et al. (12) analyzed the impact of partial ID and loss of excitation on the operational capacity of the motor. The results indicate that partial ID can affect the lifespan of the PMs and reduce efficiency. He et al. proposed a method to estimate the reduction in operational efficiency of the motor following the decrease in remanence of the PMs (13). The goal is to reflect the relationship between the complete loss of magnetization in PMSM and the resulting performance fluctuations.

The ID process leads to disadvantages and even failures in the operation of the motor. Therefore, some studies focus on predicting and diagnosing faults to proactively prevent the occurrence of ID or to address issues after ID has occurred. Moosavi et al. (14) synthesized research aimed at developing techniques for detecting demagnetization faults of PM (DFs). These faults diminish the performance, reliability, and efficiency of PMSM drive systems. Ebrahimi et al. proposed a novel method for detecting DFs caused by ID in surface-mounted PMSMs (SMPMSMs) (15). The authors suggested a theoretical analysis based on characteristics to identify DF through torque analysis. Uršič et al. (16) presented a solution for monitoring PMs in PMSM drive systems. Temperature information, along with the machine's current, is incorporated into the demagnetization model of the PMs to determine their demagnetization state. The diagnostic results for potential ID are then used to limit the opposing magnetic field to prevent ID. Pietrzak et al. (17) introduced a fault diagnosis method for DFs based on machine learning (ML) techniques for PMSM drive systems. Two ML-based models were verified and compared during the automatic detection of DFs in operation. Faiz et al. (18) compiled effective technical methods for diagnosing DFs under various operating conditions. The authors analyzed the factors causing faults in PM machines and their impact on efficiency of motor. Finally, the paper presents a general framework for developing DF diagnosis techniques under different operating conditions (static and dynamic). It can be stated that proactively diagnosing the risk of ID during operation is essential. Timely diagnosis allows operators to take appropriate measures in controlling the motor. Additionally, detecting faults due to DFs that has already occurred will enable users to take suitable actions, such as replacing magnets or the motor during operation.

Designing an appropriate motor configuration can be considered the most important step in avoiding ID. Regarding design issues, designers are now applying optimization algorithms to enhance structures that prevent temperature-induced demagnetization while still ensuring operational parameters. Yong-min et al. (19) optimized the shape of a PMSM for electric vehicles by considering the ID characteristics of PMs through a design of experiments (DOE) approach. The paper employs a multi-objective genetic algorithm to minimize the ID rate and maximize the average torque, with constraints on efficiency and torque ripple. Huang et al. (20) analyzed the ID of PMSM used in electric power steering (EPS) systems. The dimensions of the PM were optimized, taking into account magnetic loss performance and production costs. Dandan et al. (21) focused on three main issues: PM material and manufacturing technology, optimizing the electromagnetic design of the motor structure, and examining the operating environment along with necessary preventive measures against ID. Kang et al. (22) proposed an optimal rotor structure that can prevent ID of PMs in spoke-type PMSMs. Thus, research

applying various methods and algorithms in the design of PMs is diverse and serves as a crucial measure to prevent ID during the motor design phase.

In addition to applying optimization algorithms in design, studies also consider proposing motor configurations, primarily rotor configurations, that can prevent ID. Wang et al. (7) proposed a V-shaped combined pole interior PMSM (VCP-IPMSM), in which NdFeB PMs at the outer ends of the V-poles are replaced with ferrite magnets. The authors concluded that compared to traditional IPMSMs, the VCP-IPMSM configuration demonstrates improved magnetic field quality in the air gap and enhanced resistance to ID at high temperatures. Yu et al. (11) analyzed the ID characteristics of NdFeB PMs configured in a 'W' shape for LSPMSMs. The study results indicate that the risk points for ID occur at the corners of the PMs. Kim et al. (23) examined ID of PMs for three rotor types of IPMSMs. The three types of rotors are arranged with PMs in a single layer, V-shape, and double layer, commonly used for PMSMs. Choi et al. (24) investigated the ID of PMs in the rotor of various PM configurations to identify designs with higher resistance to demagnetization. Experimental results confirmed that both localized and global demagnetization can be accurately predicted using finite element analysis (FEA) over time steps. Mahmouditabar et al. (25) studied the dynamic demagnetization process for V-shaped IPMSM, conducting research on two different types of PMs. Thus, along with the application of optimization algorithms in design, the selection of PM configurations is also a key factor in preventing ID.

In addition to diagnostic studies, DF detection, and the selection of appropriate configurations in design to prevent ID, recent research has focused on proposing new methods for studying ID processes. In these studies, the factors of demagnetization and temperature are considered simultaneously. Baranski et al. presented a 2D magnetic-field-electric-circuit model that combines mechanical and thermoelectric phenomena of a LSPMSM (4). This paper applies the proposed model to investigate the demagnetization process of the motor. Zawilak et al. suggested using a magnetic circuit model of electromagnetic phenomena to analyze the demagnetization process, taking into account the effect of temperature on the characteristics of the nonlinear voltage-current and its resistance to ID (10). Jia et al. (26) studied the interaction between electromagnetic fields and thermal fields within the same motor. Additionally, the iron loss curves at different frequencies of electrical steel and the B-H curves at various temperatures of PM were used to establish the electromagnetic model of the PMSM. Palangar et al. compared electromagnetic and thermal characteristics between a LSPMSM with an external magnetic field-LSPMSM and one with an internal magnetic field-LSPMSM (5). In this study, a parameterized thermal network analysis model was proposed to analyze the thermal behavior of the two motors. Thus, it can be stated that research on ID, considering the temperature of PMSMs, has been undertaken. These studies confirm that temperature and ID are two critical factors in the operation of the motor, and these factors need to be examined together to prevent the occurrence of ID in the PMs.

Although many studies have investigated the impact of temperature on PMSMs, research on LSPMSMs, which have specific starting mechanisms and combine squirrel cage with PMs, remains limited. Unlike PMSMs, which are typically accompanied by a inverter that results in a small starting current, the LSPMSM can be directly started from the grid due to its squirrel cage rotor, eliminating the need for an accompanying inverter. Consequently, the starting current is significantly larger, being 5 to 7 times the rated current. This leads to the risk of an ID process in the LSPMSM during startup that is distinctly different from that of a PMSM.

The quantitative relationships between temperature of the starting current, demagnetization levels, and variations in electromagnetic parameters have not been fully clarified. Therefore, to study ID and its mitigation in LSPMSMs from the design phase, this paper evaluates the impact of temperature on electromagnetic parameters and analyzes its effect on ID of PMs in LSPMSM during startup. The research results are based on a theoretical model, simulated using FEA software, as well as experimental evaluations in the laboratory. The findings will provide a scientific basis for designing, operating, and maintaining LSPMSMs under extreme temperature conditions, contributing to enhanced efficiency and lifespan of the motors.

2. MATHEMATICAL MODEL OF LSPMSM CONSIDERING TEMPERATURE

When considering the effects of temperature, the mathematical model must be expanded to reflect the changes in resistance, magnetic flux, and torque due to thermal effects (27). As the temperature increases, the resistance of the stator and rotor also rises. The temperature variation is determined by the following formula:

$$\begin{aligned} R_s(T) &= R_{s0}\left[1+\alpha_s(T-T_0)\right] \\ R_r(T) &= R_{r0}\left[1+\alpha_r(T-T_0)\right] \end{aligned} \quad (1)$$

where R_s, R_r are the stator and rotor resistances at temperature T, R_{s0}, R_{r0} are the stator and rotor resistances at temperature T_0, α is the thermal expansion coefficient.

When the temperature changes, it leads to a change in the magnetic permeability of the PM material, causing the inductances, L_{md} and L_{mq}, to decrease with

temperature. In the case of no magnetic saturation, L_{md} and L_{mq} are determined by the following equations:

$$\begin{aligned} L_{md}(T) &= L_{md}(T_0)\left[1-\alpha_L(T-T_0)\right] \\ L_{mq}(T) &= L_{mq}(T_0)\left[1-\alpha_L(T-T_0)\right] \end{aligned} \quad (2)$$

where α_L is the coefficient of inductance variation with temperature (typically around α_L = 0.0005 to 0.0015/°C depending on the type of magnetic core material). L_{ls} is only slightly affected by temperature, primarily through the physical expansion of the winding. Under the assumption of linearization, the variation of L_{ls} with respect to temperature T is modeled as follows:

$$L_{ls}(T) = L_{ls}(T_0)\left[1+\alpha_{ls}(T-T_0)\right] \quad (3)$$

where α_{ls} is the coefficient of leakage inductance variation with temperature (typically α_{ls}=0.0001 to 0.0005/°C).

The mathematical model of LSPMSM considering the effects of temperature is presented as follows:

$$\begin{cases} u_{ds} = r_1(T)i_{ds} + \dfrac{d\Psi_{ds}(T)}{dt} - \omega_r.\Psi_{qs}(T) \\ u_{qs} = r_1(T)i_{qs} + \dfrac{d\Psi_{qs}(T)}{dt} + \omega_r.\Psi_{ds}(T) \end{cases} \quad (4)$$

$$\begin{cases} u'_{dr} = r'_{dr}(T)i'_{dr}(T) + \dfrac{d\Psi'_{dr}(T)}{dt} = 0 \\ u'_{qr} = r'_{qr}(T)i'_{qr}(T) + \dfrac{d\Psi'_{qr}(T)}{dt} = 0 \end{cases} \quad (5)$$

$$\begin{cases} \Psi_{ds}(T) = (L_{ls}(T) + L_{md}(T))i_{ds} \\ \qquad\qquad + L_{md}(T)i'_{dr} + \Psi'_m(T) \\ \Psi_{qs}(T) = (L_{ls}(T) + L_{mq}(T))i_{qs} \\ \qquad\qquad + L_{mq}(T)i'_{qr} \end{cases} \quad (6)$$

$$\begin{cases} \Psi'_{dr}(T) = L'_{lr}(T)i'_{dr} + L_{md}(T)(i_{ds} + i'_{dr}) + \Psi'_m(T) \\ \Psi'_{qr}(T) = L'_{lr}(T)i'_{qr} + L_{mq}(T)(i_{qs} + i'_{qr}) \end{cases} \quad (7)$$

where ω_r is the rotor angular velocity, i_{ds}, i_{qs} are the stator current of d, q axes, i'_{dr}, i'_{qr} are the rotor equivalent current of d, q axes. $\Psi_m(T)$ *is the* stator flux generated by the PMs, $L_{ls}(T)$ is the leakage inductance of the stator winding, $L_{md}(T)$ and $L_{mq}(T)$ are the magnetizing inductances of d, q axes with respect to temperature.

The mathematical model shows that under the influence of temperature, the electromagnetic parameters of LSPMSM change with varying degrees of significance. Additionally, since LSPMSM has PMs, temperature not only affects the electromagnetic parameters during operation but also has the potential to partially or completely ID of the PMs, leading to a reduction or total loss of magnetic properties. Analyzing the extent of temperature's impact on electromagnetic parameters, as well as the ID capability, is crucial for developing appropriate design and operational strategies.

3. ANALYSIS OF THE IMPACT OF TEMPERATURE ON THE DEMAGNETIZATION IN LSPMSM

3. 1. Demagnetization Mechanism of PMs Considering Operating Temperature

The demagnetization characteristic is the most important property of PMs. The relationship between load line (current) and demagnetization characteristics with respect to temperature for the NdFeB-N38 meterial is described as shown in Figure 1 (28).

The demagnetization characteristic of PMs in the second quadrant is typically represented in two forms: *B(H)* or *J(H)*. On the demagnetization curve, there exists a "knee" point, point a, at a temperature of 20°C. As the temperature increases, the demagnetization characteristic shifts to the right, and the "knee" points also move upward, corresponding to points b, c, d and k at temperatures of 60°C, 80°C, 100°C and 120^{0}C, respectively. The variation of the "knee" point on the demagnetization characteristic of the PM (shown in red) can be expressed by the equation:

$$B_{knee} = \beta H_{knee} + B_k \quad (8)$$

where B_k is the magnetic field strength. β is the slope of the “knee” characteristic with respect to temperature.

When the LSPMSM is operating, the normal working point on the demagnetization characteristic is the point of maximum energy product, which is the intersection of the

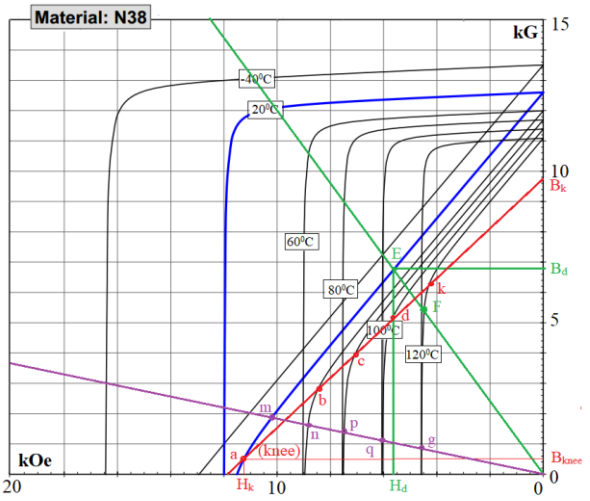

Figure 1. Demagnetization characteristics of NdFeB-N38

load line with the demagnetization curve. The remanence of the PM at the working point is determined by the equation:

$$B_d = B_r + \mu_r \mu_0 H_d \tag{9}$$

where B_d is the magnetic flux density, B_r is the remanence, H_d is the demagnetizing field μ_0 is the vacuum permeability and μ_r is the relative permeability. Demagnetization occurs when the remanence of the PM B_d is less than the remanence at the "knee" point:

$$B_d \le B_{knee} \tag{10}$$

When the motor starts, the starting current increases, causing the load line to shift downward toward the horizontal axis (shown in purple). The remanence of the PM during motor startup (point m at 20°C) is the intersection of the load line and the demagnetization curve. If the temperature of the PM increases, the remanence of the PM during startup changes to points n, p, q and g, corresponding to temperatures of 60°C, 80°C, 100°C, and 120^0C, respectively. The remanence characteristic of the PM varies with the starting current and the temperature of the magnet, as expressed by the equation:

$$B_s \le \gamma H_s \tag{11}$$

where γ is the coefficient related to the magnitude of the starting current, and H_s is the magnetic field strength generated by the stator current during startup. For NdFeB material, if partial ID occurs, then $B_s \le B_{knee}$, meaning that the limit of the magnetic field strength generated by the stator current, considering the effects of temperature, must be maintained to prevent ID:

$$\gamma H_s \le \beta H_{knee} + H_k \tag{12}$$

The starting current multiplier to avoid demagnetization for PMs, considering the effects of temperature:

$$\gamma = \beta \frac{H_{knee}}{H_s} + \frac{H_k}{H_s} \tag{13}$$

Equations 8, 9 and 10 indicate the temperature-dependent demagnetization conditions of the PMs on the demagnetization curve (Figure 1). From Equation 13 and Figure 1, it is evident that demagnetization in PMs is highly dependent on temperature. As the temperature increases, demagnetization can occur even when the LSPMSM is operating at rated load. When the LSPMSM starts, the load line shifts downward, and as the temperature rises, the "knee" point moves upward, making demagnetization more likely to occur. A suitable starting current must be defined for each operating temperature of the LSPMSM to prevent ID in PMs. Therefore, during the design process, the dimensions of the PM must be selected to ensure a correlation between current and temperature to avoid ID.

3. 2. The Effect of Temperature on the Operating Characteristics of the LSPMSM In the design of LSPMSM motors, the motor dimensions are typically selected preliminarily through analytical formulas. The initial calculation of the magnet dimensions is determined using a formula for volume. The volume of the magnet is defined by the Equation 1:

$$V_M = \frac{2.k_{of}.k_{fd}.(1+k_{EC}).P_2}{\pi^2.\xi.2.p.f.B_r.H_C} \tag{14}$$

where P_2 is the output power, f is the input frequency, B_r is the remanence, H_c is the coercive force, k_{ocf} is the overload capacity factor, k_{fd} is the magnetization form factor, k_{EC} is the electromotive force factor, ξ is the magnet utilization factor.

Typically, the thickness of the PM must be ensured according to the following equation to prevent ID, as analyzed above (29):

$$I.\frac{m}{2}.\frac{4}{\pi}.\frac{\sqrt{2}.N.k_w}{2.p.H_C} \le l_M \tag{15}$$

where m is the number of phases, p is the number of poles, I is the peak current value during startup, N is the number of stator windings, and k_w is the winding coefficient.

However, not considering the effects of temperature may be a shortcoming in this equation. This can lead to distorted operating characteristics of the LSPMSM. As the temperature increases, it not only reduces the magnetic flux generated by the PM but can also cause partial ID during operation, especially during the startup phase.

When considering the effects of temperature, the magnetic flux through the stator winding generated by the PM is determined (1):

$$\Psi_m = \frac{4Dl_s k_{w1} N}{\pi p} \sin\left(\frac{\lambda\pi}{2}\right) B_{r0}\left(1-\alpha\Delta T\right) \tag{16}$$

where D is the inner diameter of the stator, l_s is the length of the stator core, and λ is the magnetic pole coefficients.

In the case of elevated temperatures, if the PM experiences partial ID, the magnetic field generated by the magnet continues to decrease. Let ε be the coefficient of partial ID then the magnetic field generated by the PM can be determined by the following equation:

$$B_r \le \varepsilon B_{r0} \tag{17}$$

The magnetic flux linkage of the stator winding generated by the PM, taking into account the temperature and the partial ID of the PM, is determined by:

$$\Psi_m = \frac{4Dl_s k_{w1} N}{\pi p} \sin\left(\frac{\lambda\pi}{2}\right) \varepsilon B_{r0}\left(1-\alpha\Delta T\right) \quad (18)$$

The back-electromotive force (B-EMF) is determined through the magnetic flux Ψ_m as follows (32):

$$E_0 = \frac{2\pi}{\sqrt{2}} f \frac{4Dl_s k_{w1} N}{\pi p} \sin\left(\frac{\lambda\pi}{2}\right) \times \varepsilon B_{r0}\left(1-\alpha\Delta T\right) \quad (19)$$

The electromagnetic torque of the LSPMSM is defined.

$$T_{el} = \frac{3p}{2}\left[\underbrace{\left(L_{md}(T) i'_{dr} i_{qs} - L_{mq}(T) i'_{qr} i_{ds}\right)}_{T_{Ind}} + \underbrace{\Psi'_m(T) i_{qs}}_{T_{Exc}} + \underbrace{(L_{md}(T) - L_{mq}(T)) i_{ds} i_{qs}}_{T_{rel}}\right] \quad (20)$$

where T_{ind}, T_{exc} and T_{rel} are the induction, excitation and reluctance torque component with respect to temperature. The torque equation of the motor:

$$J\frac{d\omega_r}{dt} = T_{rel}(T) - T_L - B\omega_r \quad (21)$$

where T_{rel}, T_L, B, and J are the electromagnetic and load torques, friction coefficient, and inertia with respect to temperature.

In addition to temperature, the partial ID also reduces the B_r of the PMs, leading to a decrease in magnetic flux within the magnetic circuit of the LSPMSM, as described by Equation 16. This, in turn, affects the operating characteristics of the motor, which have been indicated by Equations 19, 20, and 21. From the analysis above, it can be seen that an increase in temperature alters the electromagnetic parameters of the LSPMSM, and there may also be a phenomenon of partial ID of the PM. This affects working parameters such as synchronous speed, B-EMF, and many other parameters of the LSPMSM. Neglecting the influence of temperature in the design calculations of the LSPMSM is a shortcoming that may lead to an impact on the operational characteristics of the LSPMSM.

4. SIMULATING THE EFFECT OF TEMPERATURE ON DEMAGNETIZATION DURING THE STARTUP

The report evaluates the influence of temperature on partial ID and the operating parameters of the LSPMSM, 15 kW, 3000 rpm, which has been modified from a similar IM motor with preliminary design calculations for the dimensions shown in Table 1. The main parameters related to the configuration of the motor considered are the inner diameter, outer diameter, number of slots and the core material of the rotor and stator. Additionally, the dimensions of the PM are determined using the formulas 14 and 15 as mentioned above. The length of the PM is defined to be equal to the length of the stator and rotor iron cores. The supply parameters are determined based on the supply from the corresponding induction motors.

TABLE 1. Parameters of experimental LSPMSM-15kW

Parameters	Symbol	Value	Unit
Stator outer, inner diameter	D_{in}, D_{out}	245, 152	mm
Rotor outer and shaft diameter	D, D_t	151, 52	mm
Number of stator, rotor slots	Z_1, Z_2	36, 28	slots
Air gap length	g	0,5	mm
Power supply voltage	V_n	380/660	V
Power supply frequency	f	50	Hz
Steel material	M800-50A		
Permanent magnet material	NdFeB-N38M		
PM dimensions	W x H x L	35x9x170	mm

The temperature distribution in the motor is not uniform, with certain points exhibiting the highest temperatures. During the startup process, the current of the motor increases; however, the heating time of the motor is short, preventing the thermal state from reaching equilibrium. Therefore, the study scenario in the paper assumes that the points with the highest temperatures are 20°C (equal to ambient temperature), 60°C, and 120°C, corresponding to the temperature values on the demagnetization curves of the PMs for analysis.

The paper employs the FEA to simulate the operational characteristics of the LSPMSM under varying temperature conditions. The structure of the LSPMSM, with design parameters outlined in Table 1, is constructed using FEA software, as illustrated in Figure 2. The simulation scenarios investigated involve operating the motor at temperatures of 20°C, 60°C, and 120°C. This scenario is utilized to simulate and evaluate the working characteristics of the LSPMSM.

4. 1. The Effect of Temperature on Speed Characteristics Speed characteristics are one of the important characteristics of motors. This characteristic is

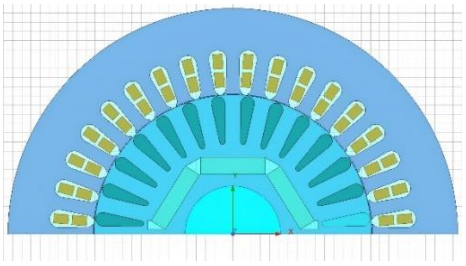

Figure 2. Configuration of LSPMSM 15kW, 2p=2

often used to assess the starting capability and quality of the motor. When the temperature changes, the speed characteristics of the LSPMSM are obtained as shown in Figure 3.

The results in Figure 3 indicate that at a temperature of 20°C, the LSPMSM starts smoothly and easily. As the temperature increases to 60°C, the starting characteristics of the LSPMSM deteriorate compared to those at 20°C due to the temperature effect. At a temperature of 120°C, the high temperature leads to partial ID of the PMs, causing the LSPMSM to lose its synchronization and operate unstably. The analysis of the starting characteristics based on temperature is summarized in Table 2.

The results in Table 2 clearly show the significant impact of temperature on the starting parameters of the LSPMSM. As the temperature increases from 20°C to 60°C, the parameters change noticeably, with the synchronization time increasing by Δt_{st}=0.13s, the oscillation time increasing by Δt_{fl}=0.2s, and the amplitude of oscillation increasing by $\Delta\omega$=50rpm. When the temperature rises further to 120°C, in addition to the impact of temperature, the phenomenon of demagnetization also affects the LSPMSM, causing it to operate unstably at synchronous speed. This instability can lead to significant vibrations, potentially resulting in motor damage.

4. 2. The Effect of Temperature on Current Characteristics Alongside speed characteristics, current characteristics are also an important attribute of motors. This characteristic is often used to assess performance, particularly the transient current. The current characteristics under three temperature conditions studied are presented in Figure 4.

In Figure 4, it can be seen that as the temperature varies at levels of 20°C, 60°C, and 120°C, the current characteristics change and differ significantly. The parameters of the current for each temperature case are presented in Table 3.

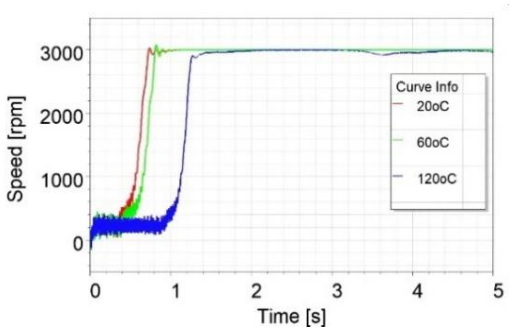

Figure 3. Configuration of LSPMSM 15kW, 2p=2

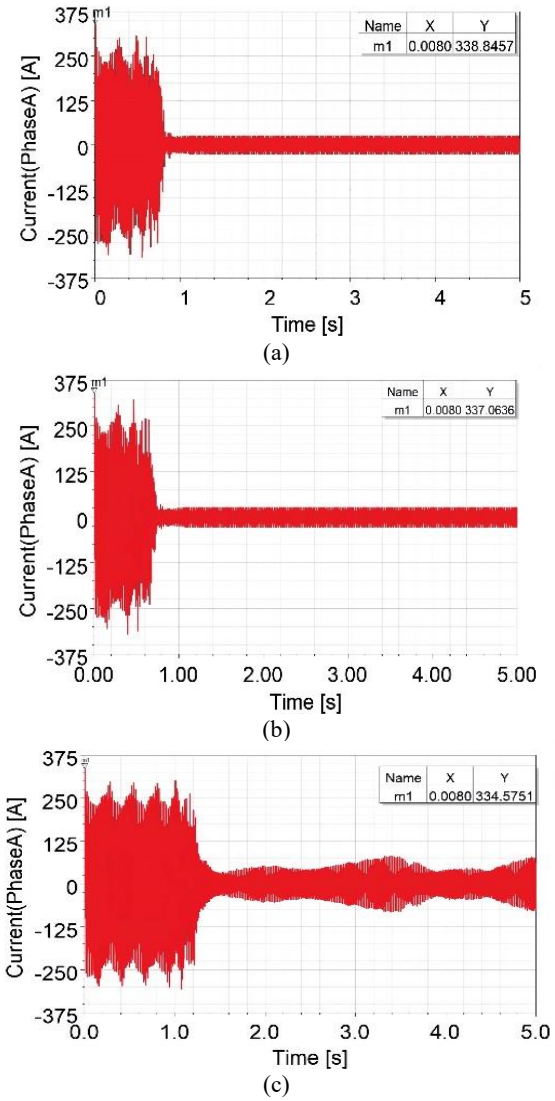

Figure 4. Simulated current characteristics at (a) 20°C, (b) 60°C and (c) 120°C.

TABLE 2. Starting parameters based on temperature

No	$T(^0C)$	Synchronous time t_{st} (s)	Fluctuation time t_{fl} (s)	$\Delta\omega_{max}$ (rpm)
1	20^0C	1.41	0.6	25
2	60^0C	1.54	0.8	75
3	120^0C	Undefined	Undefined	Undefined

TABLE 3. Current based on temperature

No.	$T(^0C)$	Fluctuation time t_{fl} (s)	Maximum starting current (A)
1	20^0C	0.6	338.A
2	60^0C	0.8	337.1
3	120^0C	Undefined	334.6

The results show that the maximum starting current in all cases is approximately 337A, which is due to the fact that the motor operates in an asynchronous state during startup. Additionally, it is observed that at temperatures from 20°C to 60°C, the starting characteristics of the motor do not differ significantly in terms of time and the maximum starting current value. However, when the temperature reaches 120°C, the time required for the motor to start and reach synchronous speed for the first time becomes very large. Once it reaches synchronous speed for the first time, the motor is also unable to operate stably as in the previous two cases. This can be explained by the fact that at a temperature of 120°C, the phenomenon of partial ID has appeared during startup. The flux generated by the PMs undergoes significant changes instead of minor changes as in the case without partial ID, and this process repeats after a few cycles until the operating point of the magnets reaches a new equilibrium state. Therefore, when starting at high temperatures, the time to reach synchronous speed for the first time is much greater. Moreover, due to the partial ID when reaching the new equilibrium state, the coercive force H_c of the PMs is significantly reduced. At this point, even a weak external magnetic field generated by the stator current can considerably alter the operating point of the magnets. This leads to strong fluctuations in the operating current once the motor reaches synchronous speed for the first time. If the LSPMSM continues to operate, leading to a further increase in temperature above 120°C, it may result in complete ID of the PMs, potentially destroying them when the temperature reaches the Curie point.

4. 3. The Effect of Temperature on B-EMF The scenario evaluates the effect of temperature and starting current on B-EMF characteristics by applying a current with an amplitude of '0' to the stator winding of the LSPMSM for the first cycle, then increasing the current amplitude to reach a value equal to the peak current when the motor starts, which is 337.8A, maintained for a second cycle. After 40ms, the phase currents A, B, and C are turned off to observe the recovery process from the remanence of the PMs and the impact of partial ID on the B-EMF characteristics corresponding to operating temperatures of 20°C, 60°C, and 120°C. The current characteristics applied to the stator windings in the simulation are shown in Figure 5.

Under the influence of the current mentioned in Figure 5, the B-EMF characteristics obtained during the simulation at corresponding temperatures of 20°C, 60°C, and 120°C are shown in Figure 6.

Figure 6 shows that the B-EMF characteristics exhibit distinct differences. In the time interval from 0 to 20 ms, when no current is applied to the stator winding, the B-EMF characteristics generated by the PMs at temperatures of 20°C, 60°C, and 120°C have a nearly sinusoidal shape and similar amplitudes. In the interval from 20 to 40 ms, when a current with an amplitude of 337.8A is applied to the stator winding, the amplitude of

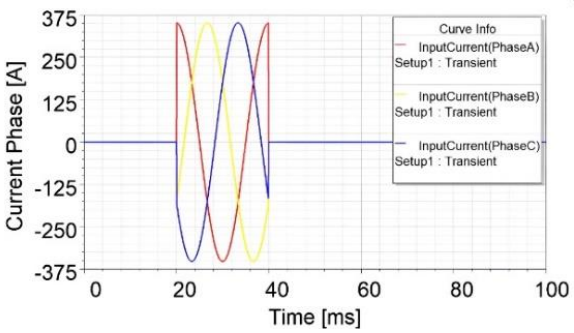

Figure 5. Current scenario in demagnetization simulation

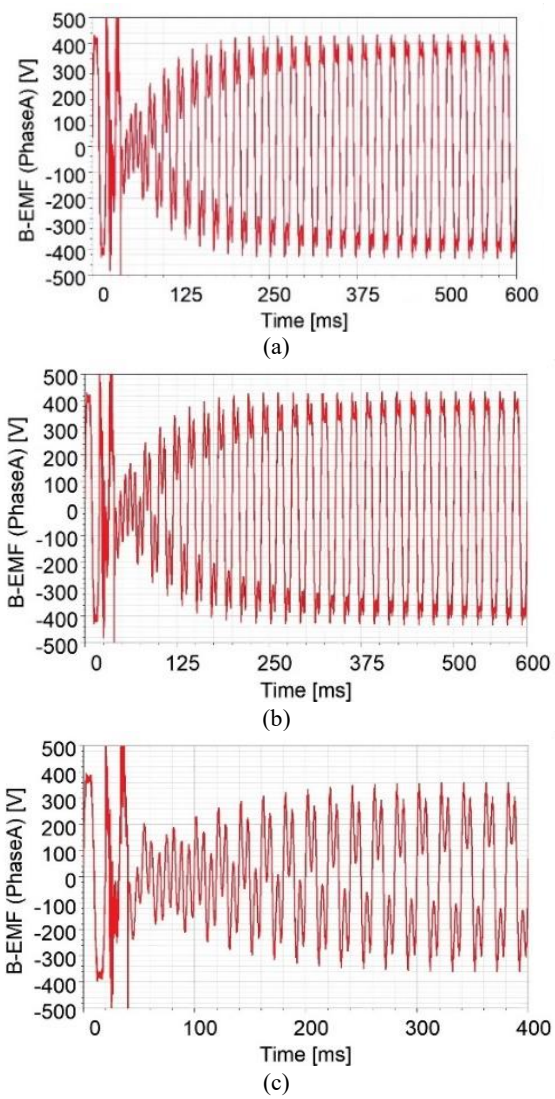

Figure 6. Simulated current characteristics at (a) 20°C, (b) 60°C and (c) 120°C.

the B-EMF decreases under the influence of the current and temperature, with the least reduction at 20°C and the most significant at 120°C. However, after removing the current from the stator at 40 ms, the amplitude of the B-EMF at 20°C is fully restored, the B-EMF amplitude at 60°C decreases slightly due to the thermal effects, and the B-EMF at 120°C shows a pronounced reduction, indicating that under the influence of the high temperature of 120°C and the large starting current of 337.8A, the PMs have experienced partial ID.

The simulation results of the waveforms at the t=0÷20ms (without applying an external magnetic field) and t=380÷400ms are presented. The interval of 380÷400 ms represents the time when the B-EMF waveform generated by the PM magnetic field recovers to a stable value in all cases considered. The waveforms for one cycle at the two time points are shown in Figure 7.

The results shown in Figure 7 (a) indicate that during the t=0÷20ms, when no external magnetic field is applied, the B-EMF waveform generated by the PMs, despite exhibiting many notches due to the influence of the teeth, stator slots, and rotor, remains fundamentally close to a sine wave. During this period, under the influence of temperature, the B-EMF characteristics decrease slitghtly at 120°C; however, the level of reduction is not significant. This can be explained by the fact that as the temperature increases, the remanence of the PMs decreases, leading to a reduction in B-EMF, which is entirely consistent with the theory presented above.

The results shown in Figure 7(b) illustrate the impact of the external magnetic field generated by the stator current during the time t=20÷40 ms on the partial ID of the PMs. Examining the B-EMF waveform at the time t=380÷400ms reveals that when operating at a temperature of 20°C, the B-EMF has fully recovered to its original shape. This indicates that partial ID of the PMs does not occur at this temperature. At 60°C, the B-EMF waveform shows a slight reduction, with the amplitude not returning to its original shape, demonstrating that at 60°C, the PMs have undergone partial ID due to the simulated starting current. At 120°C, the B-EMF waveform is significantly altered, exhibiting a dip in the middle of each half-cycle (from 360V to 120V). This indicates that substantially partial ID of the PMs has occurred under the simulation conditions. Thus, these simulation results validate the theory of partial ID dependent on the external magnetic field generated by the stator current and the operating temperature of the PMs, as analyzed above.

The B-EMF waveform was analyzed using FFT for evaluation. The B-EMF waveforms analyzed using FFT in two cases at the time t=0÷20ms and 380÷400ms are shown in Figure 8.

The $\Delta E\%$ is the measure of deviation between the amplitude value of the fundamental waveform and the

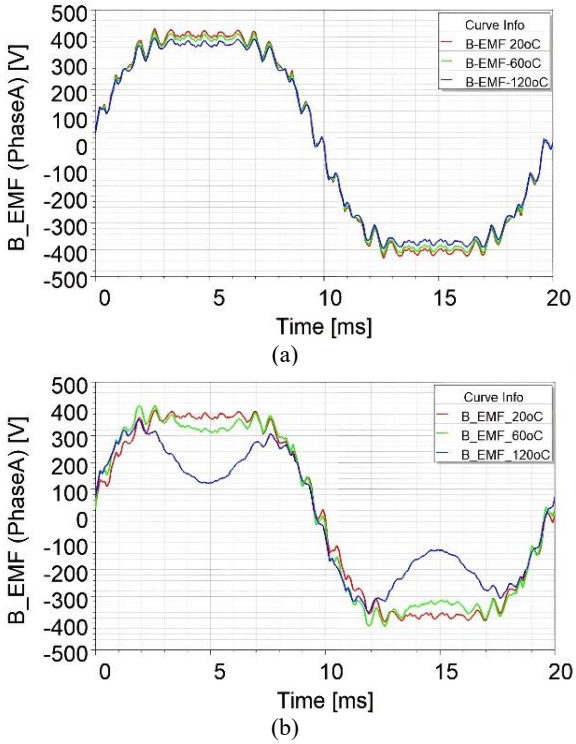

Figure 7. B-EMF waveforms at the times (a) t=0÷20ms, (b) t=380÷400ms

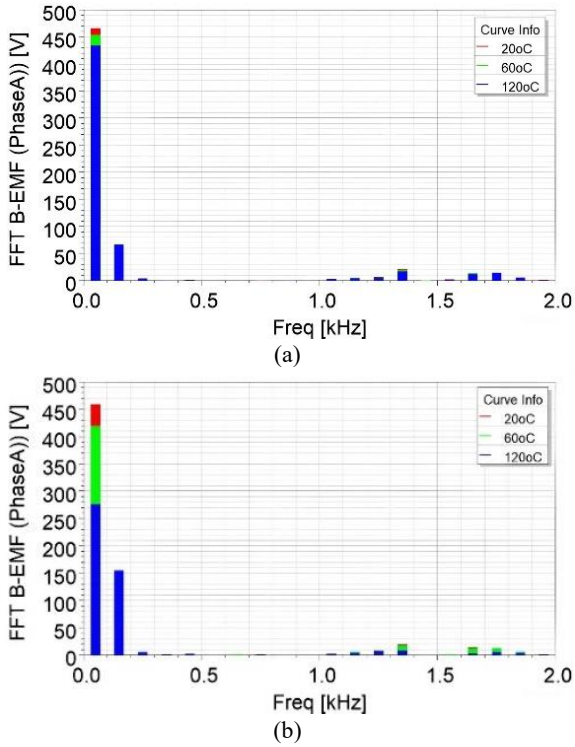

Figure 8. FFT expansion of the B-EMF waveform at the times (a) t=0÷20ms, (b) t=380÷400ms

nominal phase voltage of the power system. *ΔE%* is expressed (1):

$$\Delta E\% = \left| \frac{E_{1NB} - 380}{E_{1NB}} 100\% \right| \quad (22)$$

where E_{1NB} is the amplitude value of the fundamental waveform of B-EMF waveform. The calculation results of *ΔE%* are in Table 4.

FFT analysis of the B-EMF waveform at the time t=0÷20ms shows that the fundamental waveform decreases gradually, while the third harmonic waveform increases with temperature. Concurrently, the difference between the amplitude value of the fundamental waveform and the nominal phase voltage also increases with temperature. This can be explained by the fact that as the temperature rises, the magnetic field of the PMs decreases, leading to changes in the harmonic components of the B-EMF. During the time t=380÷400ms at a temperature of 20°C, the amplitude of the fundamental waveform remains constant. At 60°C, ΔE% increases and reaches a value of 28.2%. At 120°C, ΔE% increases significantly to 94.7%, which is due to the severely partial ID of PMs at high temperatures.

5. DEMAGNETIZATION EXPERIMENT OF LSPMSM

The author team constructed a LSPMSM 15 kW, 2p=2 for experimentation in the laboratory. The LSPMSM was tested to analyze and evaluate the impact of temperature on motor operation. The rotor structure and the experimental model are shown in Figure 9.

TABLE 4. ΔE% at different operating temperatures

T(°C)	*t*=0÷20ms		*t*=380÷400ms	
	E_{1NB}	*ΔE%*	E_{1NB}	*ΔE%*
20°C	328	15.9	328	15.9
60°C	320	18.6	296	28.2
120°C	306	23.8	195	94.7

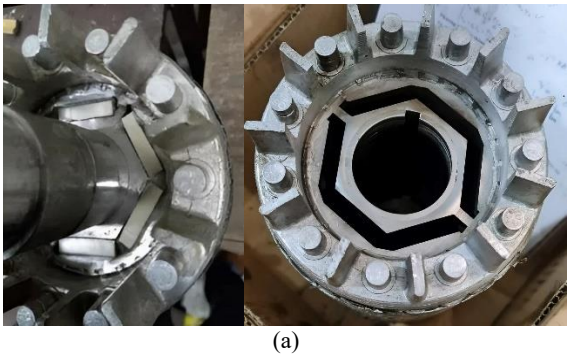

(a)

(b)

Figure 9. Rotor and testing model of LSPMSM 15kW (a) rotor configuration, (b) testing model

The PMs are considered the source of magnetic flux (self-excitation) for the LSPMSM. If the PMs undergo demagnetization, the B-EMF of the LSPMSM will be reduced in both amplitude and sinusoidal shape. The testing scenario is conducted in two steps:

Step 1: Perform the motor starting test at a laboratory temperature of 20°C.

Step 2: Start the LSPMSM under high-temperature conditions. Due to the difficulty of heating the motor and considering that the LSPMSM is custom-built and will be used in several subsequent studies, heating the motor to 120°C could damage other components and lead to motor failure. Therefore, to avoid damaging the motor while still being able to investigate partial ID, the author group examined the motor with a temperature increase up to 60°C.

The prototype motor was fabricated and tested to validate the theoretical research and simulations presented. However, due to limitations in experimental conditions, only two cases at temperatures of 20°C and 60°C were conducted for comparison with the simulation results.

The operating temperature of the motor is controlled through the measured winding resistance. The heating process is carried out by operating the motor under rated load for a sufficient duration, with the cooling fan removed. The motor self-heats to reach approximately 60°C before stopping. After that, the motor is started to investigate the B-EMF characteristics. The results of the EMF characteristics when the LSPMSM starts at a temperature of 60°C are shown in Figure 10.

The experimental results shown in Figure 10, when the motor starts at a room temperature of 60°C, indicate that the B-EMF characteristics exhibit a concave peak shape, similar to that shown in Figure 7(b) when simulating the LSPMSM starting at a temperature of 60°C. This demonstrates that the magnetic field of the permanent magnet has been slightly diminished and cannot be fully recovered, unlike when starting the motor at a room temperature of 20°C. Thus, the PM has experienced partial ID in this case. The analysis of the waveform when testing at room temperature of 20°C and at 60°C is provided in Table 5.

(a) (b)

Figure 10. B-EMF waveform at temperatures (a) 20°C (b) 60°C

TABLE 5. Comparison of testing results and simulation

$T(^0C)$	20^0C	60^0C
E_{1NB}(V) - Simulation	328	296
E_{1NB}(V) - Testing	306	279

The results in Table 5 and Figures 10 show that there is a similarity in the B-EMF waveforms between the experimental results and the simulation results at room temperatures of 20°C and 60°C, with an error of less than 7%. The simulation results and experimental results are also fully consistent with the previously analyzed theory. This demonstrates that temperature has a significant impact on the demagnetization phenomenon of permanent magnets. To ensure the magnetic properties of the LSPMSM during operation, it is essential to consider the temperature factor and select an appropriate type of PM with a strong magnetic field and high-temperature tolerance to provide a reserve against partial ID.

6. CONCLUSION

The study has shown that temperature is a key factor affecting the demagnetization phenomenon and operational parameters of a LSPMSM. The increase in temperature during startup or under heavy load not only degrades the magnetic properties of the PMs but also affects the electromagnetic parameters of the LSPMSM, particularly concerning partial ID during motor startup. When partial ID occurs, the motor will operate with parameters that do not meet the required specifications, potentially even performing worse than an induction motor of the same power rating.

The theoretical research results indicate that, under certain temperature conditions, there exists a maximum starting current coefficient to prevent partial ID. Using FEA for a LSPMSM 15 kW, 2-pole the results showed consistency between theory and simulation, demonstrating that with a high starting current of 337.8 A, the NdFeB-N38M magnets used in the motor can experience mild demagnetization at 60°C, with pronounced partial ID occurring at 120°C. When partial ID occurs at 120°C, the LSPMSM loses synchronization and operates in an unstable mode, leading to increased current and a sudden drop in the B-EMF.

Additionally, the author group also constructed a testing LSPMSM of 15 kW, 2p=2 for experimental purposes. The results indicated that at normal operating temperatures, the B-EMF waveforms were consistent across theoretical, simulated, and experimental results. The experimental results confirmed the accuracy of the B-EMF waveforms, showing a similarity in shape between experimental and simulation data with an error of less than 7%.

The research results indicate that when operating at high temperatures, the theoretical formulas for selecting the dimensions of the PMs may no longer be accurate. partial ID can occur even when the LSPMSM is operating under rated load. When the LSPMSM starts, the load current drops, while the temperature increases, leading to a higher likelihood of partial ID. An appropriate starting current must be defined for each working temperature of the LSPMSM to prevent ID of the PMs. Therefore, during the design process, the dimensions of the PMs must ensure a correlation between current and temperature to avoid partial ID.

Thus, high-temperature resistant materials of PMs can be used to avoid partial ID; however, this will result in increased costs. Additionally, the electromagnetic circuit design can be optimized to reduce the starting current, or magnetic barriers can be employed to adjust the external magnetic field applied to the PMs in the rotor's magnetic circuit.

Funding

The authors declare that no financial support was received for this study.

Ethics Approval and Consent to Participate

This article does not involve any studies with human participants or animals performed by any of the authors. Therefore, ethics approval and consent to participate are not applicable.

Competing Interests

The authors declare no financial or organizational conflicts of interest.

Data Availability

The data that support the findings of this study are available upon reasonable request.

Authors Biosketches

Le Anh Tuan is a lecturer in the field of Electrical Engineering, currently working at the SEEE, HaUI,

Vietnam. He received his Ph.D. in Electrical Engineering from HUST, Vietnam, in 2018. His research areas include electric machines, electric machine simulation and electrical switching devices.

Tran Duy Khanh is a Lecturer in the Department of Electrical Engineering at Sao Do University (SDU), Vietnam. He is currently pursuing the Ph.D. degree in Electrical Engineering at Hanoi University of Mining and Geology, with a research focus on line-start permanent magnet synchronous motors (LSPMSMs).

Do Nhu Y received Ph.D. degree in Electrical Engineering in 2013 from Tula State University, Russia. He is the Head of the Department of Electrification and Deputy Director of the Center for Mine Electromechanical Research at the University of Mining and Geology (HUMG). His research interests include electric machines, power quality and renewable energy.

REFERENCES

1. Le AT, Lan NT, Do NY, Bun HV. Studying the effect of PM thickness on the back-EMF and power factor of LSPMSM. Journal Européen des Systèmes Automatisés. 2025;58(3):493-500. https://doi.org/10.18280/jesa.580307
2. Cepoi RD, Jaşcău FF, Szabó L. Current trends in energy efficient electrical machines. Journal of Electrical and Electronics Engineering. 2017;10(2):13-18.
3. Chaudhari M, Chowdhury A. Improved performance analysis of single-phase line start synchronous reluctance motor derived from induction motor. International Journal of Engineering, Transactions B: Applications. 2022;35(8):1641-50. https://doi.org/10.5829/ije.2022.35.08b.20
4. Baranski M, Szelag W, Jedryczka C. Influence of temperature on partial demagnetization of the permanent magnets during starting process of line start permanent magnet synchronous motor. In: International Symposium on Electrical Machines (SME); 2017. p. 1-6. https://doi.org/10.1109/ISEM.2017.7993535
5. Palangar MF, Soong WL, Mahmoudi A. Outer and inner rotor line-start permanent-magnet synchronous motors: an electromagnetic and thermal comparison study. In: IEEE Energy Conversion Congress and Exposition (ECCE); 2021. p. 1-8. https://doi.org/10.1109/ECCE47101.2021.9595574
6. Quoc VD, Huu HB. Modeling of surface-mounted permanent magnet synchronous motors with inner and outer rotor types. International Journal of Engineering, Transactions C: Aspects. 2024;37(12):2529-37. https://doi.org/10.5829/ije.2024.37.12c.11
7. Wang M, Zhu H, Zhou C, Zheng P, Tong C. Analysis and optimization of a V-shape combined pole interior permanent-magnet synchronous machine with temperature rise and demagnetization considered. IEEE Access. 2021;9:64761-75. https://doi.org/10.1109/ACCESS.2021.3076228
8. Faiza J, Rafieib V. Design of a three-phase outer rotor synchronous motor for hybrid vehicle. International Journal of Engineering, Transactions B: Applications. 2024;37(11):2380-91. https://doi.org/10.5829/ije.2024.37.11b.22
9. Gherabi Z, Toumi D, Benouzza N, Bendiabdellah A. A proposed approach for separation between short circuit fault, magnetic saturation phenomenon and supply unbalance in permanent magnet synchronous motor. International Journal of Engineering, Transactions A: Basics. 2020;33(10):1968-77. https://doi.org/10.5829/ije.2020.33.10a.15
10. Zawilak T, Jędryczka C. Risk of irreversible demagnetisation under transient states of the line start permanent magnet synchronous motor taking into account magnet temperature. Archives of Electrical Engineering. 2023;72(4):1107-19. https://doi.org/10.24425/aee.2023.147429
11. Yu P, Zhu C, Shen Y, Zhang G. Demagnetization analysis of line-start permanent magnet synchronous motors during its starting process. In: International Conference on Electrical, Automation and Mechanical Engineering (EAME); 2018. p. 1-6. https://doi.org/10.2991/eame-18.2018.11
12. Adly AA, Huzayyin A. The impact of demagnetization on the feasibility of permanent magnet synchronous motors in industry applications. Journal of Advanced Research. 2019;17:103-8. https://doi.org/10.1016/j.jare.2019.02.002
13. He H, Zhou N, Sun C. Efficiency decrease estimation of a permanent magnet synchronous machine with demagnetization faults. Energy Procedia. 2017;105:2718-24. https://doi.org/10.1016/j.egypro.2017.03.922
14. Moosavi SS, Djerdir A, Amirat YA, Khaburi DA. Demagnetization fault diagnosis in permanent magnet synchronous motors: a review of the state-of-the-art. Journal of Magnetism and Magnetic Materials. 2015;391:203-12.
15. Ebrahimi BM, Faiz J. Demagnetization fault diagnosis in surface mounted permanent magnet synchronous motors. IEEE Transactions on Magnetics. 2012;49(3):1185-92. https://doi.org/10.1109/TMAG.2012.2217978
16. Uršič L, Nemec M. Permanent magnet synchronous machine demagnetisation prevention and torque estimation control considering rotor temperature. IET Power Electronics. 2019;12(9):2161-9. https://doi.org/10.1049/iet-pel.2018.6162
17. Pietrzak P, Wolkiewicz M. Demagnetization fault diagnosis of permanent magnet synchronous motors based on stator current signal processing and machine learning algorithms. Sensors. 2023;23(4):1757. https://doi.org/10.3390/s23041757
18. Faiz J, Bazrafshan MA, Tabarniarami Z. Demagnetisation fault analysis and diagnosis based on different methods in permanent magnet machines—an overview. IET Electric Power Applications. 2024;18(12):1860-93. https://doi.org/10.1049/elp2.12519
19. You YM, Yoon KY. Multi-objective optimization of permanent magnet synchronous motor for electric vehicle considering demagnetization. Applied Sciences. 2021;11(5):2159. https://doi.org/10.3390/app11052159
20. Huang W, Wang J, Zhao J, Zhou L, Zhang Z. Demagnetization analysis and magnet design of permanent magnet synchronous motor for electric power steering applications. In: China International Youth Conference on Electrical Engineering (CIYCEE); 2020. p. 1-6. https://doi.org/10.1109/CIYCEE49808.2020.9332771
21. Dandan Q, Yanan J, Shuyang Z. The study of permanent magnet demagnetization in permanent magnet synchronous motor. In: International Conference on Advances in Electrical Engineering and Computer Applications (AEECA); 2021. p. 1-6. https://doi.org/10.1109/AEECA52519.2021.9574353
22. Kang DW. Analysis of vibration and performance considering demagnetization phenomenon of the interior permanent magnet motor. IEEE Transactions on Magnetics. 2017;53(11):1-7. https://doi.org/10.1109/TMAG.2017.2708421
23. Kim KC, Kim K, Kim HJ, Lee J. Demagnetization analysis of permanent magnets according to rotor types of interior permanent magnet synchronous motor. IEEE Transactions on Magnetics. 2009;45(6):2799-802. https://doi.org/10.1109/TMAG.2009.2018661
24. Choi G. Analysis and experimental verification of the demagnetization vulnerability in various PM synchronous

machine configurations for an EV application. Energies. 2021;14(17):5447. https://doi.org/10.3390/en14175447

25. Mahmouditabar F, Vahedi A, Ojaghlu P. Investigation of demagnetization effect in an interior V-shaped magnet synchronous motor at dynamic and static conditions. Iranian Journal of Electrical and Electronic Engineering. 2018;14(1):22-27.
26. Jia M, Hu J, Xiao F, Yang Y, Deng C. Modeling and analysis of electromagnetic field and temperature field of permanent-magnet synchronous motor for automobiles. Electronics. 2021;10(17):2173. https://doi.org/10.3390/electronics10172173
27. Bilgin O, Kazan FA. The effect of magnet temperature on speed, current and torque in PMSMs. In: International Conference on Electrical Machines (ICEM); 2016. p. 1-6. https://doi.org/10.1109/ICELMACH.2016.7732809
28. Truong Cong T, Nguyen Vu T, Bui Minh D, Vo Thanh H, Dang Quoc V. Analytical modelling of a six-phase surface mounted permanent magnet synchronous motor. International Journal of Engineering, Transactions A: Basics. 2024;37(7):1274-83.
29. Lee BH, Jung JW, Hong JP. An improved analysis method of irreversible demagnetization for a single-phase line-start permanent magnet motor. IEEE Transactions on Magnetics. 2018;54(11):1-5. https://doi.org/10.1109/TMAG.2018.282850

Persian Abstract

چکیده

موتور سنکرون آهنربای دائم با راه‌اندازی خطی (LSPMSM)به دلیل راندمان بالای خود، به طور فزاینده‌ای مورد استفاده قرار می‌گیرد. با این حال، دما تأثیر قابل توجهی بر پارامترهای الکترومغناطیسی دارد که به نوبه خود بر ویژگی‌های عملیاتی LSPMSM تأثیر می‌گذارد. به دلیل وجود اجزای قفس سنجابی در روتور، LSPMSM می‌تواند با راه‌اندازی خطی کار کند، اما جریان راه‌اندازی بالا می‌تواند منجر به مغناطیس‌زدایی موضعی یا کامل، به ویژه در دماهای بالا، شود. این امر می‌تواند منجر به مغناطیس‌زدایی برگشت‌ناپذیر آهنرباهای دائمی شود. این مقاله به بررسی تأثیر دما بر پارامترهای الکترومغناطیسی موتور و همچنین تأثیر آن بر مغناطیس‌زدایی در هنگام راه‌اندازی LSPMSM می‌پردازد. نتایج مطالعه نظری، تأثیر دما بر پارامترهای الکترومغناطیسی LSPMSM را نشان می‌دهد و نشان می‌دهد که در شرایط دمایی خاص، یک ضریب جریان راه‌اندازی حداکثری برای جلوگیری از مغناطیس‌زدایی وجود دارد. با استفاده از شبیه‌سازی FEA برای یک موتور LSPMSM با توان ۱۵ کیلووات و p=2، نتایج نشان‌دهنده‌ی همبستگی بین یافته‌های نظری و شبیه‌سازی شده است. نشان داده شده است که با جریان راه‌اندازی بالای ۳۳۷.۸ آمپر، آهنرباهای NdFeB-N38M مورد استفاده در موتور می‌توانند در دمای ۶۰ درجه سانتیگراد دچار مغناطیس‌زدایی خفیف شوند، در حالی که مغناطیس‌زدایی قابل مشاهده در دمای ۱۲۰ درجه سانتیگراد رخ می‌دهد. اعتبارسنجی تجربی، دقت را تأیید کرده است، زیرا ویژگی‌های B-EMF نشان‌دهنده‌ی شباهت نزدیک بین نتایج تجربی و شبیه‌سازی شده با انحراف کمتر از ۷٪ است.